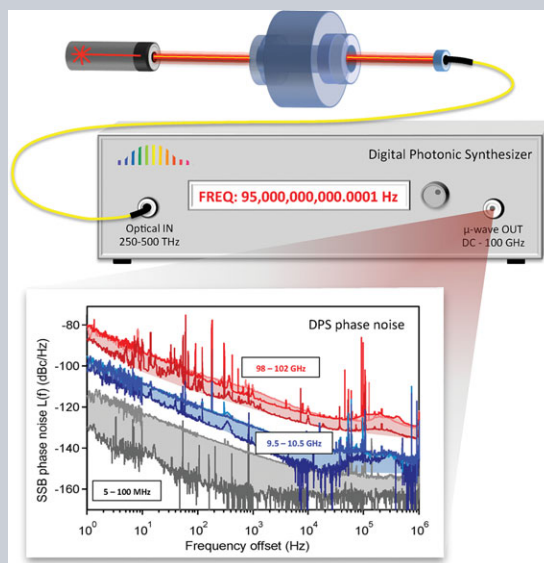ORIGINAL PAPER

Abstract Fundamental science, as well as all communications and navigation systems, are heavily reliant on the phase, timing, and synchronization provided by low-noise and agile frequency sources. Although research into varied photonic and electronic schemes have strived to improve upon the spectral purity of microwave and millimeter-wave signals, the reliance on conventional electronic synthesis for tuning has resulted in limited progress in broadband sources. Using a digital-photonic synthesizer architecture that derives its time-base from a high-stability optical reference cavity, we generate frequency-agile and wideband microwave signals with exceptional dynamic range and with a fractional frequency instability of 1×10^{-15} at 1 s. The presented architecture demonstrates digitally controlled, user defined and broadband frequency tuning from RF to 100 GHz with orders-of-magnitude improvement in noise performance over room-temperature electronic wide-bandwidth synthesis schemes.

Optically referenced broadband electronic synthesizer with 15 digits of resolution

T. M Fortier[1,*], A. Rolland[1,**], F. Quinlan[1], F. N. Baynes[1,**], A. J. Metcalf[2], A. Hati[1],
A. D. Ludlow[1], N. Hinkley[1], M. Shimizu[3], T. Ishibashi[3], J. C. Campbell[4], and S. A. Diddams[1]

1. Introduction

Microwave atomic references, first developed in the 1950's [1], revolutionized modern time keeping and sparked the development of high-stability microwave sources that are the cornerstone in current navigation, synchronization and communications systems. As the demands on these systems increases, so does the need for even better synthesized frequency sources. For instance, higher spectral purity signals can allow for longer coherence times in quantum information systems [2], improved resolution in opto-mechanical sensing [3] and radio-astronomy [4,5], better synchronization in large-scale science facilities [6], as well as increased dynamic range and resolution in radar and sensing [7]. Additionally, a future redefinition of the SI second based on an optical atomic clock [8] will shift the primary frequency standard out of the range of electronics, requiring a link between arbitrary RF, microwave, or millimeter-wave frequencies and optical clocks.

For more conventional electronic sources at room temperature, the best performance on the timescale of

0.01–10 s comes from oven-controlled 5 MHz quartz with a stability as good as 8×10^{-14} [9]. Further improvements in the stability of electronic oscillators on this timescale have required operation at cryogenic temperatures, with impressive achievements in Q and stability coming from quartz, niobium and sapphire dielectric resonators in the microwave X-band [10–13]. However, the improved 1 s stability typically comes at the expense of spectral purity at time-scales from 0.1–$100~\mu$s, where exceptional performance is achieved with room-temperature oscillators employing sapphire and air-dielectric cavities [14, 15]. Although frequency synthesis with these sources has been demonstrated [16, 17], there is generally a compromise between noise performance and the wideband and agile tuning desired for many applications.

As an attractive alternative, room-temperature optical frequency references can provide quality factors on the order of 10^{11} [18] (optical atomic clocks enable much higher Q's $\sim 10^{15}$ [19–21]), and the technique of optical frequency division (OFD) enables the faithful transfer of the optical frequency stability to the microwave domain

[1] NIST, Time and Frequency Division, 325 Broadway MS 847, Boulder, CO 80305, USA
[2] Purdue University, West Lafayette, IN 47907, USA
[3] NTT Electronics Corporation Naka-shi, Ibaraki-ken, 311-0122, Japan
[4] University of Virginia, 351 McCormick Road, Charlottesville, VA, USA
** A. Rolland and F.N. Baynes are now with National Physical Laboratory, Teddington, UK
*Corresponding author: E-mail: fortier@boulder.nist.gov

[22–24]. As a result, photonic generation via OFD has demonstrated enormous gains in electronic signal purity [22] over hydrogen masers, competing photonic architectures [25–27], MEMS based sources [28–30], conventional quartz-based electronics, and has demonstrated comparable performance to cryogenic electronic oscillators [11, 31].

Until now, however, optical frequency division with modelocked lasers has resulted in fixed frequency signals with very limited tuning. Here we introduce a broadband synthesizer architecture that leverages the harmonic nature of OFD and the exquisite timing of optical references to exploit the full utility and resolution of direct digital synthesis (DDS). The presented architecture represents a simple and elegant method for enabling wideband, frequency agile, and precise phase tuning of electronic signals while simultaneously supporting the frequency resolution of optical atomic clocks. Using this technique we demonstrate high fidelity transfer in frequency stability to the microwave and millimeter-wave domains, achieving frequency-agile signals with exceptional dynamic range and up to 15 digits of resolution.

2. Experimental section and methods

Figure 1 shows a conceptual depiction of our experimental technique for realization of a digital-photonic synthesizer (DPS). This Figure accompanies the more detailed experimental set up shown in Fig. 2. Below, the details of the experimental setup and techniques are broken up into two parts: Section 2.1 entails a discussion of the photonic timebase, while Section 2.2 is focused on how we use that timebase to synthesize low-noise radio frequency, X-band and W-band electronic signals.

It is important to note that in our measurements, characterization of the absolute phase noise and fractional frequency instability was obtained using two nearly identical, but independent digital-photonic synthesizers. This required duplication of the digital-photonic setup to provide a reference system with similar performance. In the sections below we describe the setup for a single system, but indicate important differences between the two systems when relevant.

2.1. The photonic timebase

A synthesizer using a time-base derived via optical frequency division (OFD) [32] offers several technical advantages over architectures based on electronic crystal oscillators. Optical reference cavities exhibit extremely low-loss and drift and thereby achieve much higher quality factors ($Q\sim10^{11}$) and consequently lower instabilities (10^{-16} at 1 s) than room-temperature electronic resonators [18, 33]. Synthesis begins with the reference in the optical domain, yielding division as opposed to multiplication of the reference noise on the derived microwave carrier. Additionally, high-linearity and high-power photodetectors
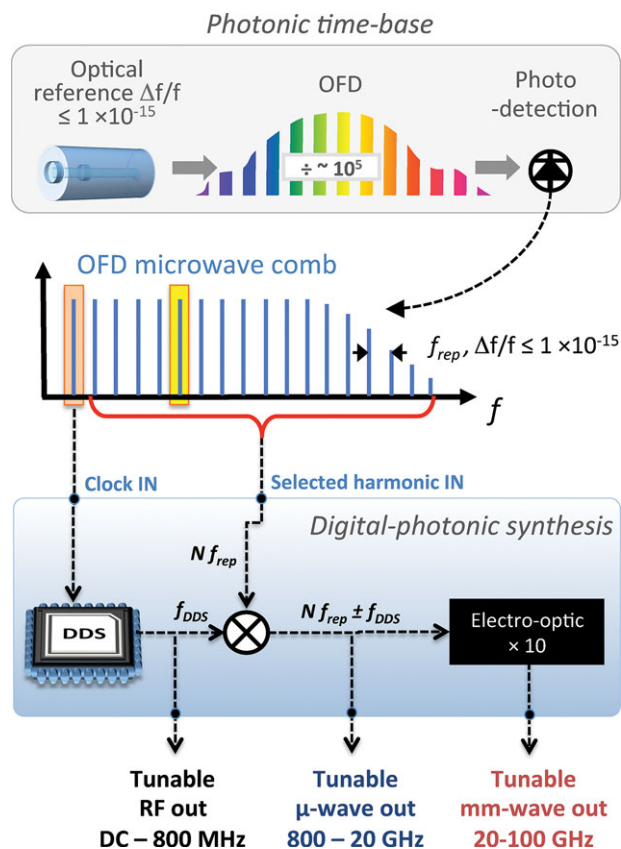

Figure 1 (A) The simplified and generalized architecture for a digital-photonic synthesizer (DPS). The microwave harmonic comb used as the timebase is generated via optical frequency division (OFD) of a high-stability optical reference cavity at 282 THz. The lowest order microwave harmonic mode at $f_{rep} = 2$ GHz clocks a direct digital synthesizer (DDS) that generates phase tunable RF frequencies from DC to 800 MHz. Electronic mixing of this RF signal with a selected harmonic, $N f_{rep}$, of the microwave comb leverages the digital synthesis range up to 20 GHz. Electro-optic multiplication by 10 of ($N f_{rep} + f_{DDS}$) enables generation of tunable mm-wave frequencies (20–100 GHz).

[34, 35], necessary for conversion of optical signals to the microwave domain, have been shown to support residual frequency instabilities of 10^{-17} at 1 s averaging on a 10 GHz carrier [36], and a phase noise floor approaching 18 orders of magnitude below the carrier [37]. While the latter noise levels are not demonstrated in the measurements presented here, continued research into these novel devices could potentially enable Watt-level microwave signals with high bandwidth, exceptional dynamic range and sub-femtosecond timing jitter.

2.1.1. Optical reference cavity

The microwave frequency comb that serves as the timebase to our synthesis architecture is derived via division by 10^5 of an ultra-stable frequency reference at 282 THz [18]. We employ two optical frequency references, one at 282
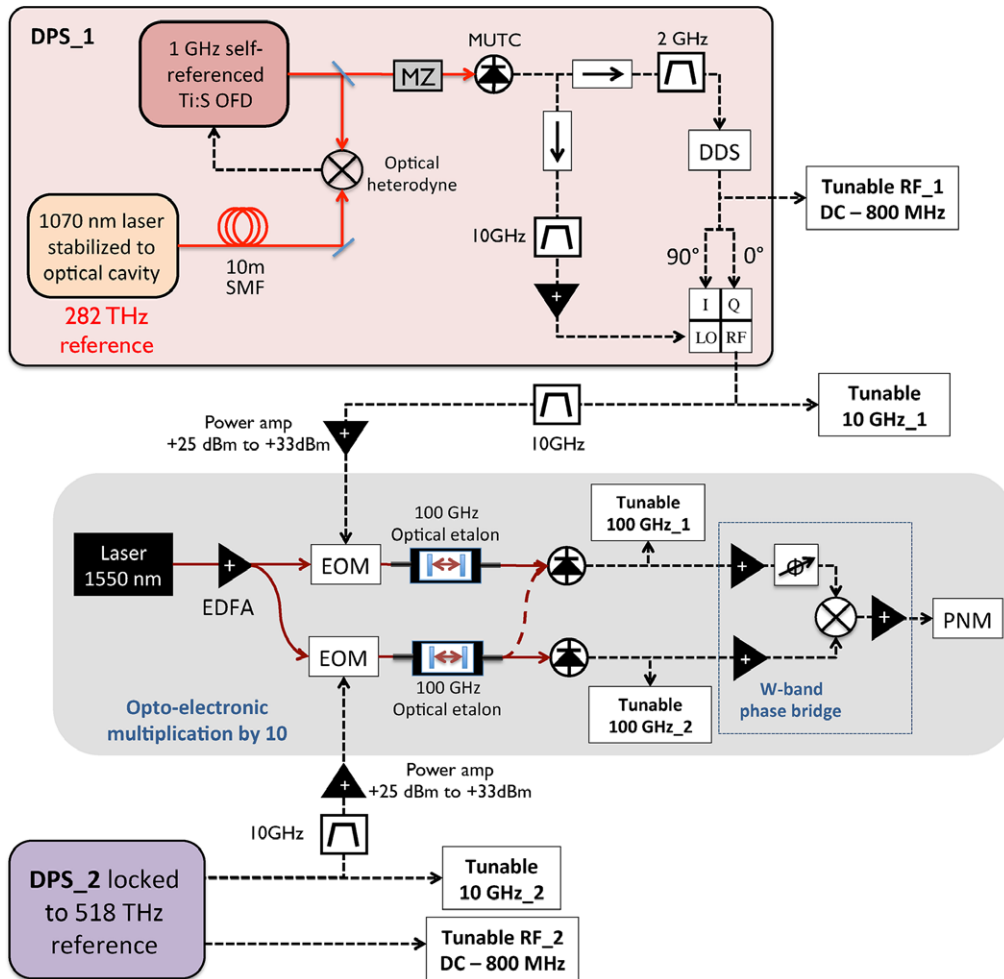
Figure 2 Experimental setup for realization and characterization of a digital-photonic synthesizer. DPS_1 is a digital-photonic synthesizer phase locked to an optical reference at 282 THz. DPS_2 is a second digital-photonic synthesizer locked to a second an independent optical reference at 518 THz. The second DPS has an identical set up to DPS_1 and is used as a reference to characterize the phase noise and fractional frequency stability of DPS_1. Also included is the W-band phase bridge used for measurement of the tunable 100 GHz phase noise and its fractional frequency stability. Characterization of the 100 GHz photodiode residual noise was obtained by taking the output of a single optical etalon and splitting it between the two 100 GHz photodetectors (see dashed dark red line in the grey inset). DPS- digital photonic synthesizer, MZ- Mach Zender pulse interleaver, PNM – phase noise measurement system, EOM- electro-optic modulator, EDFA- erbium-doped fiber amplifier, SMF – single mode fiber, MUTC-modified uni-traveling carrier photodetector.

THz [38] and the other at 518 THz [18]. The optical frequency references are passive, two-mirror optical cavities constructed with an ultra-low expansion glass ULE spacer with near zero thermal expansion at room temperature. The optical cavity is held in a temperature-controlled vacuum chamber to isolate it from environmental perturbations, and the cavity is mounted such that acceleration of the cavity is minimally coupled to changes in length. With appropriate isolation, the cavity can exhibit an impressively small absolute length changes that averaged over 1 s are less than the diameter of an atomic nucleus (∼1 femtometer). An intensity-stabilized, single-frequency laser is locked to a single longitudinal mode of the optical reference cavity via and electro-optic modulation using a Pound-Drever Hall stabilization scheme [39]. The cavity stabilized light is

delivered via noise-cancelled optical fiber [40] to the mode-locked laser that enables division of the optical carrier to the microwave domain. Ideally, division of the 282 THz (518 THz) optical carrier to 10 GHz or 100 GHz also reduces the optical phase noise power spectral density by the division factor squared, or conversely, by 89 dB (92 dB) or 69 dB (72 dB), respectively.

2.1.2. Optical frequency comb divider

In our experiments we used two optical frequency comb dividers based on passively mode-locked octave spanning Ti:Sapphire lasers [41], both with a native repetition rate of 1 GHz (pulse period of 1 ns, round trip cavity length

of 30 cm). Each laser produced greater than 1 W average power with a usable optical bandwidth direct from the laser that spans 600 –1200 nm. It is important to note that similar performance can be achieved with an Er:fiber laser with some additional optical engineering to account for the lower native repetition rate, optical power and narrower optical bandwidth [42]. Because the optical frequency comb is a pulsed laser, its optical frequency spectrum is composed of several hundred thousand phase related, coherent and equidistant optical modes. The spectrum of this "optical comb" is characterized by only two RF frequencies, the laser repetition rate, f_{rep}, that determines the comb spacing, and the laser offset frequency, f_o, that determines the comb offset from zero. Any optical mode, N, of the comb can then be described as $\nu_N = f_o + N f_{rep}$. The optical spectrum of an OFD is stabilized by acting on the laser cavity length using a piezo-actuated mirror, and by changing the laser gain via an acousto-optic modulator actuating on the laser pump power. This allows for control of the laser repetition rate and the laser offset frequency, respectively. The laser-offset frequency is measured using the technique of self-referencing described in Ref. [43]. The OFD spectrum is stabilized to the optical reference via optical heterodyne with the cavity-stabilized laser described above [44]. This generates a RF beat note that measures the difference between a single comb line and the cavity-stabilized laser. Feeding back to the cavity length of the OFD to stabilize the frequency of the optical beat signal against a synthesized RF frequency transfers the stability of the optical reference to every optical mode of the OFD. The coherent addition of the optical modes required for modelocking, translates this frequency stability to timing stability of the emitted laser pulse train, such that the pulse-to-pulse timing jitter is less than 1 femtosecond. The conversion of the optical pulse train to a microwave signal is obtained via opto-electronic conversion with an optical photodetector.

2.1.3. Optical photodetection

The frequency spectrum of the derived electronic signal from the photodetector is a stable microwave comb composed of equally spaced harmonic tones separated by the pulse repetition rate, f_{rep}. The optical photodetector in our experiments are based on a modified uni-traveling carrier (MUTC) photodetector design that is optimized for high power handling, high speed, and high linearity [45]. Upon photodetection the optical pulse train is converted to a train of stable electronic pulses that carry the timing and stability of the optical pulse train, but with some loss in dynamic range at higher offset frequencies [46]. Pulse interleaving of the optical pulse train effectively multiplies the native pulse repetition rate from 1 GHz to 2 GHz, which alleviates nonlinearities in photodetection by reducing the energy per pulse [47]. Additionally, the photodiode is operated in a regime whereby its response is most linear, at very high bias voltage (−21V) and at a low photocurrent for the device (18 mA), which minimizes the effects of amplitude to phase noise conversion. At this bias voltage and photocurrent

level we extracted a 10 GHz microwave signal strength of +8 dBm directly from the photodiode. Harmonics at lower frequency exhibited similar or slightly higher carrier strengths.

2.2. Digital-photonic synthesis

Since optical frequency division provides high spectral purity microwaves only at predetermined frequencies, it cannot directly produce arbitrary, frequency agile, user-defined frequencies as required of a synthesizer of the broadest utility. Some agility of the microwave comb is possible by tuning the repetition rate of the optical pulse train, but this tends to be slow and limited to 1–2% due to stability constraints of the mode-locked laser cavity [48]. A combination of OFD and regenerative frequency division can yield RF signals with extremely low-noise [32], but this does not enable frequency tuning.

A direct digital synthesizer (DDS) offers an attractive approach to synthesis because a single clock input enables digitally generated signals with fast slew rates (<1 μs), precise phase tuning and low residual noise [49]. In more traditional DDS-based synthesis schemes, however, the signal purity is overwhelmed by the timing error of the input clock signal, typically quartz-based. Additionally, the bandwidth of the DDS is typically less than 2 GHz, limited to less than 50% of the input clock frequency. Thus, access to higher frequencies requires multiplication of the DDS-derived RF signal, and consequently the input clock noise. In contrast, the 2 GHz clock supplied via OFD provides a timing stability that is 100 times better than conventional oven-controlled quartz, and 20 times better than the best oven-controlled BVA quartz [9]. This enables DDS derived RF signals whose timing jitter is limited only by the digital electronics.

Furthermore, here we overcome the bandwidth limitations in DDS by leveraging the harmonics of the OFD microwave comb to extend the digital synthesis range. By up- or down-shifting the frequency of any OFD harmonic, $N f_{rep}$, using a single sideband mixer by up to $f_{DDS} = \pm f_{rep}/2$, we can generate any frequency from near DC up to the highest harmonic detected from the OFD. Aside from allowing the potential for continuous tuning, using this digital-photonic synthesis architecture, the electronic noise added by the DDS is additive, not multiplicative.

2.2.1. Radio frequency digital-photonic synthesis

In our measurements, we employed a DDS (Analog Devices 9914[1] evaluation kit) with 64-bit frequency tuning, corresponding to a pHz frequency resolution. The evaluation kit included an analog-to-digital converter, a DDS and a digital-to-analog converter (DAC). The DDS was clocked

---

[1] Any use of trade, firm, or product names is for descriptive purposes only and does not imply endorsement by the U.S. Government.

with the lowest order harmonic at 2 GHz from the OFD. When clocked at 2 GHz, the DDS could synthesize a tunable analog signal, f_{DDS}, from near DC up to 800 MHz. As mentioned previously, the RF signals derived from the DDS are entirely limited by the noise of the evaluation kit, that yields an excess residual instability of approximately 2×10^{-14} at a 1 s averaging time.

2.2.2. X-band digital-photonic synthesis

Although the residual noise of the DDS in generating RF signals can be impressively low, its specified instability of 10^{-14} at 1 s averaging is still an order of magnitude higher than that supported by the optical reference. As mentioned previously, when using the DDS to shift the frequency of the microwave comb harmonics, the noise in DDS is additive. Based on the DDS specifications we know that, the close-to-carrier residual noise in DDS becomes comparable to that of OFD for harmonics close to 10 GHz. As a result, tuning of the OFD harmonics at 10 GHz and above should enable derivation of signals with the stability and spectral purity limited mainly by the performance of the optical reference.

To further verify this concept we demonstrate the performance of the synthesizer when the 10 GHz OFD harmonic is combined with the DDS output to produce a low noise, tunable X-band signal. As seen in the lower portion of Fig. 1, generation of the agile 10 GHz signal is obtained by combining the $N = 5$ harmonic at 10 GHz from the OFD harmonic spectrum with the synthesized output from the DDS using a single sideband mixer [5]. This frequency converter has 3 input ports (I, Q, and LO), and one output port, RF. The LO port is driven at $+10$ dBm with the 10 GHz from the OFD. Ideally, by driving the I and Q ports in quadrature and with equal amplitude at f_{DDS}, the IQ mixer produces one strong tone at 10 GHz $+ \mathbf{f_{DDS}}$ and suppresses both the LO signal at 10 GHz and the image frequency at 10 GHz $- \mathbf{f_{DDS}}$. By switching the phases of the I and Q ports by 90 degrees one can choose which image signal is suppressed. For simplicity a broadband hybrid coupler (5-500 MHz) was employed to split the signal from the DDS input to the I and Q ports of the mixer, which limited our synthesized X-band bandwidth to 9.5–10.5 GHz. Although the amplitude and phase at the output of the hybrid coupler was not perfectly balanced, we observed suppression of the local oscillator and image signals by approximately 30 dB. Careful control of the phase and amplitude to the I and Q ports of the SSB mixer could significantly improve the suppression of the image frequency, and small DC offsets into the I and Q ports can improve rejection of the LO signal.

Characterization of the synthesized X-band signals output from the DPS_1 was compared to the reference DPS, DPS_2, using a double balanced X-band mixer. In our phase noise measurements, the difference frequency between the two tunable 10 GHz signals was always maintained at a difference frequency of 25 MHz. This intermediate frequency was input to a Symmetricom 5125A[1] phase
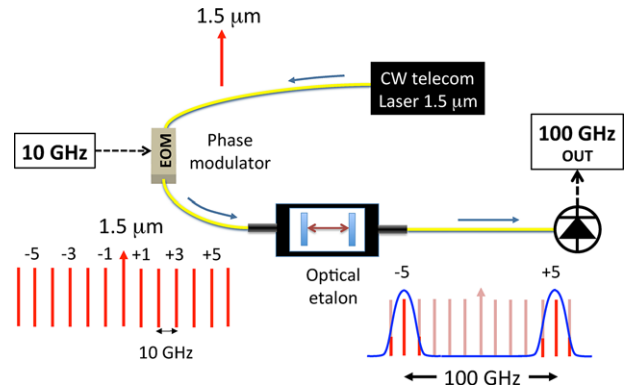

Figure 3 Conceptual description of the experimental setup for opto-electronic multiplication of 10 GHz signals to 100 GHz. Sidebands spaced by 10 GHz from the X-band DPS are modulated onto a 1.5 μm laser with an electro-optic modulator (EOM) driven by the 10 GHz from the DPS. An optical etalon is used to filter two 100 GHz spaced optical modes for efficient photodetection of a 100 GHz electrical signal.

noise analyzer for measurement of the phase noise and fractional frequency stability. A low noise 5 MHz quartz oscillator was used as a stable reference for phase noise and frequency counting measurements (5 MHz phase noise of -120 dBc/Hz at 1 Hz offset).

2.2.3. W-band digital-photonic synthesis

Extension of digital-photonic synthesis to higher microwave frequencies can be achieved via several different schemes. Electronic multiplication can be employed to convert X-band signals to the W-band [50, 51]. While this method is adequate for quartz-based synthesizers, it would degrade the spectral purity and limit the high-frequency noise floor of our DPS microwave signals. An additional drawback of electronic multiplication is that it does not allow for efficient distribution of W-band signals. In our approach described below we employ electro-optic multiplication of X-band signals derived via our DPS to enable both low-noise synthesis of W-band signals and efficient fiber-optic distribution. The latter has immediate applications to radio-over-fiber [52] and at large scale facilities such as free-electron laser centers, as well as in radio-astronomy.

As seen in Fig. 3 we achieve 10 times optical multiplication of our 10 GHz DPS signal by phase modulating a continuous wave (CW) laser at 1550 nm with an electro-optic modulator (EOM) [53–57]. For generation and comparison of agile 100 GHz signals, we employed low-loss EOMs, each driven by independent 10 GHz signals with carrier strengths between 25–30 dBm. The EOMs were used to phase modulate a single 20 mW, 1.5 μm CW laser. Prior to being split between the two EOMs, the laser was amplified to 200 mW using a polarization maintaining Er-doped fiber amplifier. Both EOMs were overdriven by the agile 10 GHz signals, producing multiple phase modulation sidebands (up to greater than ± 5 about the CW optical carrier). The

modulated CW laser was then centered midway between the modes of a fixed frequency 100 GHz spaced optical etalon, each with a 10 GHz optical linewidth. Consequently, the etalon only passed harmonics with the order +5 and −5, yielding two optical lines separated by 100 GHz, with an average optical power of 15 mW, and with residual 10 GHz sidebands -10 dB down from the optical carrier. Although the tuning range in our current setup is limited to 98–102 GHz due to the passband of the optical etalon, agility over a larger band should be possible with a tunable optical etalon or a reconfigurable optical filter. Photodetection of the optically-filtered and DPS-modulated 1550 nm laser with two NEL[1], W-band UTC photodiodes [58], biased at −2 V and directly coupled to a WR10 waveguide, enabled us to extract a 100 GHz carrier of -5 dBm (5 mA photocurrent) from each photodetector.

Once the tunable 100 GHz signals were generated, characterization of the phase noise and fractional frequency stability was obtained using a W-band phase bridge built from waveguide components. As seen in Figure 2, in the light grey shaded area, the W-band phase bridge compares the two optically-generated 100 GHz electronic signals by driving the RF and LO ports of a W-band double balanced mixer. Both branches of the phase bridge required amplification for proper operation of the mixer. A low-noise amplifier was used in the RF branch to drive the RF port of the mixer at 0 dBm and a power amplifier was used to drive the LO port of the mixer at +15 dBm. The intermediate frequency output from the W-band mixer at 50 MHz was filtered and amplified and then input to a Symmetricom phase noise test set to evaluate the phase noise and frequency stability.

In our measurements we also characterized the noise contribution of the electro-optic multiplication setup. Evaluation of the W-band photodetectors and opto-electronic multiplication setup residual noise, required that the W-band phase bridge to be driven in quadrature. The two 100 GHz signals were generated by splitting the optical signal after one of the 100 GHz etalons and illuminating both UTC photodiodes. A phase shifter in the RF branch of the phase bridge was used to place the signals in quadrature. The DC signal output from the mixer was then amplified with a low noise IF amplifier and the combined phase noise measured with vector signal analyzer with a bandwidth of 10 MHz.

3. Results and discussion

Figure 4 shows the results of the characterization of the RF, X-band and W-band signals generated using the digital-photonic techniques described in Section 2. Evaluation of the signal phase noise allows for an evaluation of the synthesizer spectral purity. In the measurements presented below, the noise spectra are presented as the noise spectral density in a 1 Hz bandwidth, normalized to the microwave carrier. For instance, a noise level of −120 dBc/Hz at a 10 Hz offset demonstrates that the noise sideband in a 1 Hz bandwidth on the oscillator, 10 Hz from the carrier are 10 orders of magnitude below the peak of the carrier. Integration over
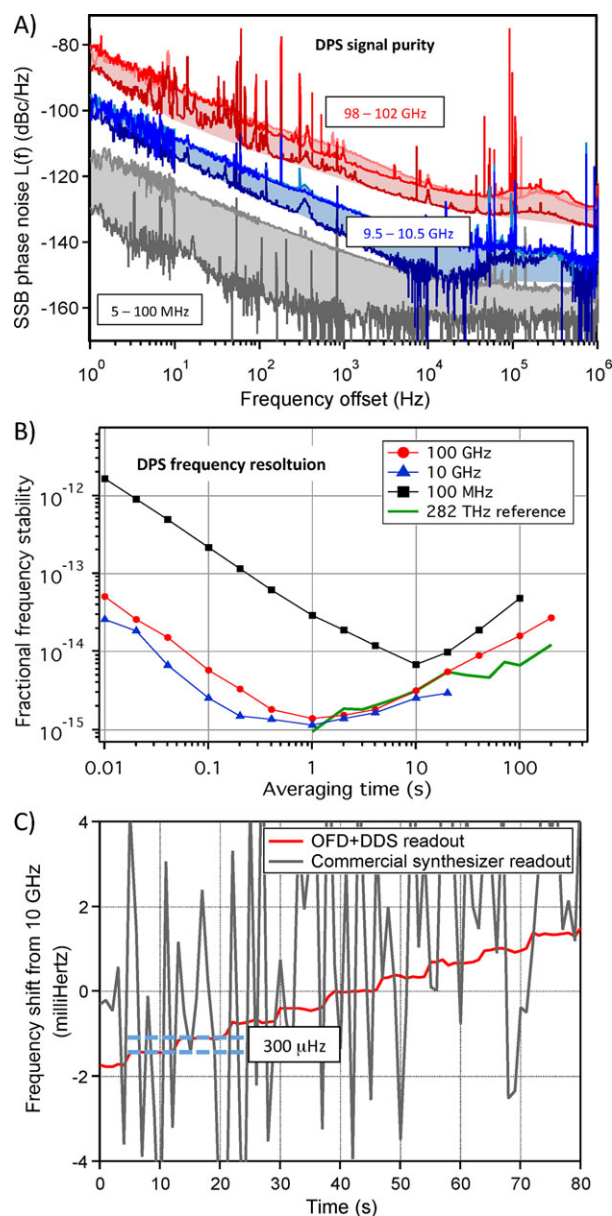

Figure 4 (A) Absolute phase noise of synthesized digital-photonic signals. The measurement shows the level of the noise sidebands relative to the stated carrier frequencies in a 1 Hz bandwidth. For the signals synthesized from 5–100 MHz, the noise is lowest at 5 MHz and increases until the top of the band at 100 MHz. For synthesized signals about 10 and 100 GHz, the noise increases with tuning away from the unshifted harmonics at 10 and 100 GHz. (B) Optical reference cavity and DPS-derived RF, microwave and mm-wave signals stability versus averaging time. C) Readout of a stepped 10 GHz DPS source with (grey line) a H-maser referenced synthesizer and (red line) a second 10 GHz DPS source counted with a 1 s gate time. The standard deviation in the frequency at each step was approximately 23 μHz.

the noise spectra from 1 Hz to Niquist enable determination of the oscillator timing jitter.

It is important to note that all the measurements presented below of the frequency resolution and spectral purity

show the combined phase noise and stability for two DPS systems. As a result, the reported phase noise levels are 3 dB higher, and the reported fractional frequency stabilities are up to 1.4 times greater than that of a single system, assuming both systems contribute equally.

3.1. Spectral purity in digital-photonic synthesis

Figure 4(A) shows the measured phase noise levels of signals generated via digital photonic synthesis in three frequency bands: from 5–100 MHz (RF), from 9.5–10.5 GHz (X-band), and from 98–102 GHz (W-band). For signals synthesized in the RF domain, the measured phase noise levels are entirely limited by the noise of the DDS since perfect division of the 2 GHz clock signal to 5 MHz would support a close-to-carrier phase noise level at a 1 Hz offset of less than -165 dBc/Hz, and a noise floor below -200 dBc/Hz. As a result, the observed phase noise in the lowest frequency bands perfectly match those of the expected DDS $1/f$ noise and the quantization noise in the 12-bit DAC used in the DDS evaluation kit. A better DAC could offer a lower noise floor and improve the signal timing jitter.

Figure 4(A) also shows the results of the absolute phase noise of the synthesized signals from 9.5 GHz to 10.5 GHz. In Fig. 4(A) we see that the phase noise of the un-shifted 10 GHz harmonic is -105 dBc/Hz at a 1 Hz offset from the carrier, falling to a close to -150 dBc/Hz. This noise spectrum determines the OFD contribution to the DPS synthesized noise. Synthesis about this carrier with the DDS to generate frequencies between 10 GHz and 10.25 GHz, yield close-to-carrier phase noise levels comparable to that observed at 10 GHz. For tuning of the 10 GHz harmonic beyond 250 MHz, the $1/f$ noise and the quantization noise from the DDS begins to contribute to the observed phase noise levels. Consequently, the phase noise at 10.5 GHz overlaps exactly with the noise level obtained for DDS synthesis of a 500 MHz RF signal.

Finally, in Fig. 4(A), we observe the measured phase noise of the DPS generated X-band signals that are optically multiplied to the W-band signal near 100 GHz. For all synthesized signals in the band 98–102 GHz, the absolute phase noise is observed to be less than -80 dBc/Hz at 1 Hz offset. We would predict that the observed phase noise levels obtained at 100 GHz would be approximately 20 dB higher than the phase noise levels in observed in the X-band near 10 GHz, which would reflect perfect multiplication of the agile 10 GHz signals to 100 GHz. In Fig. 4(A), in the band from 98–102 GHz we observed slight deviations in the increase in phase noise by 20 dB as compared to those observed for synthesized signals near 10 GHz. This deviation most likely results from data being taken on different days, reflecting small changes in the drift of the optical reference cavities and small changes in the servo parameters for locking of the optical frequency dividers. A more rigorous evaluation of the noise in electro-optic multiplication is described later on in this section.

From our measurements in Fig. 4(A) we conclude that RF signals generated from clocking the DDS with the 2 GHz harmonic from the OFD are entirely limited by the residual noise in the DDS. Regardless of the excess noise added via the DDS evaluation kit, we observe that the DDS derived RF phase noise levels are comparable to those produced with the *best* fixed-frequency quartz oscillator, but here, with the full utility of digital synthesis. The DPS signals in the RF, however, contribute significantly less when used to shift the OFD harmonic at 10 GHz, since the noise of the OFD at 10 GHz and the residual noise of the DDS become comparable. As a result, in Fig. 4(A), we observe that the synthesized signals from 9.5 GHz to 10.5 GHz maintain a *combined* close-to-carrier noise below -97 dBc/Hz at a 1 Hz offset. Integration of the phase noise at this level from 1 Hz to 1 MHz yields an integrated timing jitter that is less than 1 femtosecond. Because we observe that electro-optic multiplication adds minimally to the noise, the integrated timing jitter on the tunable 100 GHz signals are also less than 1 femtosecond.

3.2. Achievable resolution with digital-photonic synthesis

Figure 4(B) shows the fractional frequency stability of the synthesized signals obtained with the digital photonic synthesizer in the RF, X-band and W-band at 100 MHz, 10 GHz and 100 GHz, respectively. Only a single frequency is shown for each band because the signals synthesized within one band exhibited the same fractional frequency stability. Also shown is the fractional frequency stability of the optical reference for comparison. From the Figure we observe that, the excess DDS noise above the "ideal" OFD noise levels increased the fractional frequency stability to $> 1 \times 10^{-14}$ at 1 s averaging. The observed fractional frequency stability determines the frequency resolution of the DPS as a function of averaging time. For instance, at RF frequencies the maximum frequency resolution at 10 s averaging time is approximately 14 digits, or 1 part in 10^{-14}. At carrier frequencies above 10 GHz, when the noise of OFD is comparable to that of the DDS, we obtain a frequency resolution of 1 part in 10^{-15} in a 1 s averaging time. At longer averaging times we observe a decrease in frequency resolution that results from the slow frequency drift (<10 Hz/s at 282 THz) of the optical cavities. At these higher frequencies, the observed phase noise levels correspond to a *combined* fractional frequency instability of less than 2×10^{-15} at 1 s averaging time reproducing the stability of the optical reference cavities.

3.3. High resolution microwave digital-photonic synthesis

As an illustration of the resolution possible with our agile X-band signals we demonstrate fine frequency stepping of the 10 GHz source. In our measurement, the output of

one DPS was incremented in 300 μHz steps. The 10 GHz stepped source from one digital-photonic synthesizer was mixed with a local oscillator near 10 GHz and the down-converted signal was counted with a gate time of 1 s. Fig. 4(C) shows the readout of the stepped signal as performed with two local oscillators; a fixed 10 GHz signal from a H-maser referenced synthesizer, and a fixed 10 GHz signal from a second DPS. From the Figure, it is only possible to resolve the fine frequency steps of the photonically generated 10 GHz signal with a second DPS since the electronically referenced synthesizer lacks the necessary frequency resolution. Although 300 μHz resolution is shown here, an advantage of our synthesis approach is that the ultimate resolution is given by the 64-bit frequency tuning of the DDS, which corresponds to sub nHz frequency resolution. On the 10 GHz carrier, this yields an ultimate frequency resolution greater than 19 digits. Low-noise and fine frequency resolution is an important attribute of this technique, whose combination can enable improved security in communications by enabling low modulation data encoding, faster carrier detection and frequency hopping [59].

3.4. Noise in electro-optic multiplication

As progress in optical atomic references and DDS technologies continue to increase their respective frequency resolutions, the noise limitations in opto-electronic frequency multiplication and mm-wave photodetection become more pertinent. Figure 5 shows a comparison between the absolute phase noise of W-band signals generated via optical and electronic multiplication of 10 GHz signals generated via DPS. Also shown is the residual noise contributed by the opto-electronic multiplication setup, including the 100 GHz phase noise measurement setup. As seen in Fig. 5, the dominant source of noise for offset frequencies from 1 Hz -1 kHz results from opto-electronic conversion in the high-speed photodetectors (green trace). From this trace we can estimate an upper limit to the flicker level of $-100\,f^{-1}$ for detection of a 100 GHz signal. The blue shaded area from 10 kHz -3 MHz indicates the noise added by the 1.5 μm CW laser, FM-to-AM conversion in the optical etalon as well as AM-to-PM conversion of the in the phase modulator (EOM). Although the EOM is driven at very high power at 10 GHz, added noise in the power amplifier is expected to predominantly affect the noise floor of the amplified 10 GHz signals via the amplifier noise figure. We believe the dominant noise source in the electro-optic multiplication setup to result from amplitude fluctuations on the 10 GHz modulation signal being converted to phase noise in the optical sidebands. Intensity stabilization of the 10 GHz drive signal could be employed in the future to minimize phase noise due to AM-to-PM in the multiplication setup. Finally, from the residual noise measurements above, we find that the opto-electronic multiplication setup can support derivation of mm-wave signals with a frequency resolution at a level of 1 part in 10^{16} at 1 s averaging.
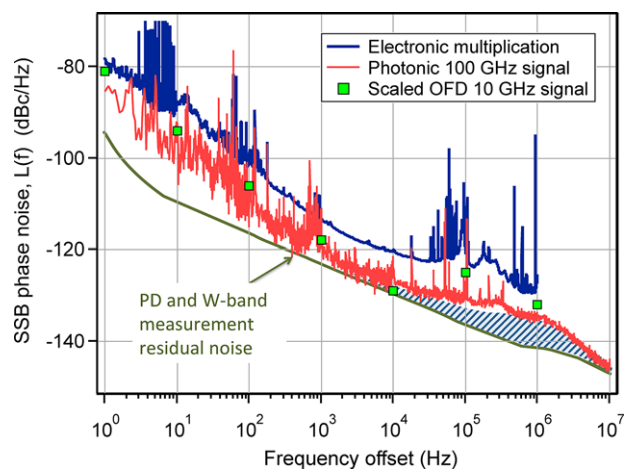

Figure 5 Characterization of noise sources at 100 GHz. Absolute phase noise of two 90 GHz signals obtained via 9 times electronic multiplication (blue trace), and two 100 GHz signals obtained via opto-electronic multiplication (red trace), of photonically generated 10 GHz signals. The green trace shows the baseline level obtained for measurement of the residual noise in photodetection at 100 GHz. The blue shaded area shows the excess noise in opto-electronic multiplication, which includes the contribution of the CW laser, the optical amplifier, the 10 GHz power amplifier, the electro-optic phase modulator and the optical etalon. The filled green squares shows the calculated 10 times multiplication of the 10 GHz phase modulator drive signal.

In principle, the technique of opto-electronic multiplication with filtering can be used to generate microwave or mm-wave signals at any multiple of the EOM drive frequency, up until the cut off of the W-band photodiode [54,55]. With higher bandwidth photodiodes [60] one could extend this approach to even higher frequencies. Aside from supporting the very low-noise possible with OFD, electro-optic modulation allows for efficient dissemination of microwave and mm-wave signals via a telecom carrier [61]. Finally, the techniques we introduce should be applicable to the generation of a low-noise microwave and millimeter wave signals with significantly improved stability for improved resolution and precision in optical arbitrary waveform generation, optical signal processing and ranging [62] [57].

3.5. Data summary: radio frequency, X-band and W-band synthesis with DPS

To put in perspective the power of microwave synthesis via optical frequency division, Fig. 6 provides a comparison of DPS synthesized electronic signals as compared to other room-temperature synthesizers. Also included is the phase noise of a fixed frequency cryogenic sapphire oscillator (CSO) at 11 GHz and the frequencies synthesized from CSOs via electronic multiplication to 103 GHz and electronic division to 10 MHz. As can be seen in Fig. 6(A), the spectral purity of our RF signals is comparable with
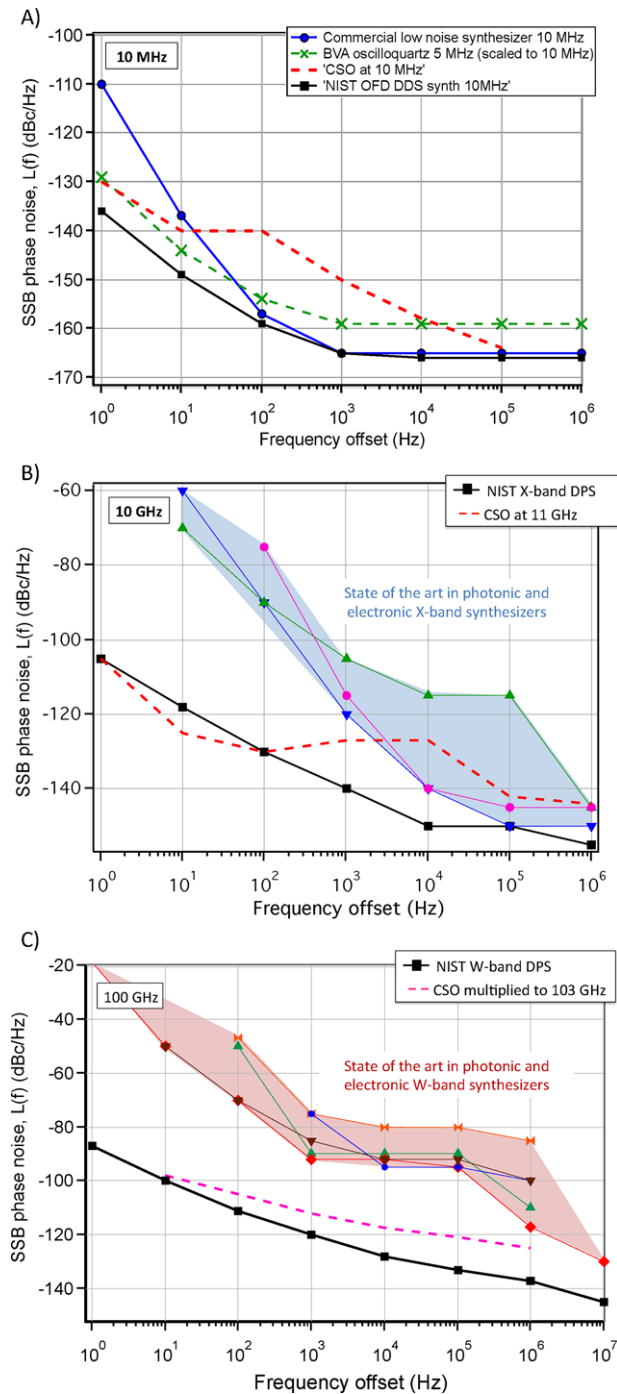
Figure 6 Single oscillator comparison of the spectral purity of tunable sources room-temperature synthesizers (markers and solid lines [55, 77, 80–84]) as compared to DPS-derived tunable signals for carrier frequencies (A) 10 MHz, (B) 10 GHz and (C) 100 GHz. Additionally we present the phase noise levels for perfect scaling of a BVA fixed quartz source at 10 MHz and the phase noise for a cryogenic electronic oscillator at 11 GHz [11] and synthesis cryogenic oscillators for derivation of fixed frequency 10 MHz [17] and 103 GHz signals [85]. The phase noise denoted by the red diamonds in (C) is achieved via 6 times electronic multiplication of 15 GHz from a commercial source.

BVA quartz and with that of the CSO but with the benefit of full digital synthesis. In the X-Band and W-band seen in Fig. 6(B) and (C), respectively we observed comparable performance to CSOs but with the added benefit of broadband tuning. And as compared to room-temperature synthesis with quartz and competing photonic techniques, we observed gains in performance (nearly a 50 dB and 70 dB improvement close to carrier at 10 GHz and 100 GHz, respectively). Although the gain in performance comes with increased complexity in the present system, our photonic approach has the potential for great reduction in form factor and cost, while achieving still better phase noise.

Currently there are significant efforts aimed at advancing the technical maturity of the key technologies of OFD such that it could be realized in real-world settings. This includes both field and flight demonstrations of fiber-based lasers and frequency combs [63–67] and ultra-stable optical reference cavities [68–70]. Packaging of advanced photodiode technology has also been demonstrated [58, 71]. Thus, our development of the DPS architecture that can interface with these systems to enable broad bandwidth and versatile electronic synthesis becomes more important. In parallel, there has been significant effort aimed at miniature low-noise lasers and optical reference cavities [72–74], which could be further combined with micro-resonator frequency combs [75, 76] to enable OFD with chip-integrated components [77], or even stand-alone clocks [78] and oscillators [79]. Such integrated systems would employ and benefit from the DPS technique we introduce here, thereby vastly extending the breadth and scope of current microwave capabilities and applications outside the laboratory.

4. Conclusions and outlook

We demonstrate ultra low-noise synthesis of agile RF, X-band, and W-band signals by a combination of electro-optic multiplication and RF digital synthesis to enable continuous electronic tuning across the microwave harmonic frequency comb generated via optical frequency division. This digital-photonic architecture enables user-defined broadband tuning with up to 15 digits of resolution for frequencies beyond 10 GHz and extending synthesis into the W-band at 100 GHz. User-defined synthesis of RF, microwave and mm-wave frequencies with the precision and stability of optical atomic references represents a significant advance in microwave synthesis with important consequences for basic science as well as military and civilian technologies. Finally, a redefinition of the primary frequency standard to an optical atomic clock will require a synthesis architecture such as this in order to link arbitrary electronic frequencies to the future SI second.

our research. This work is a contribution of the US Government and is not subject to copyright in the US.

References

[1] L. Essen and J. V. L. Parry, Philos. Trans. Royal Soc. Lond. A: Math., Phys. Eng. Sci. **250**, 45–69 (1957).

[2] J. W. Britton, B. C. Sawyer, A. C. Keith, C. C. J. Wang, J. K. Freericks, H. Uys, M. J. Biercuk, and J. J. Bollinger, Nature **484**, 489–492 (2012).

[3] L. A. De Lorenzo, and K. C. Schwab, New J. Phys. **16** (2014).

[4] J. F. Cliche, B. Shillue, C. Latrasse, M. Tetu, and L. D'Addario, in Ground-Based Telescopes, Pts 1 and 2, J. M. Oschmann, Ed. (2004), vol. 5489, pp. 1115–1126.

[5] N. R. Nand, J. G. Hartnett, E. N. Ivanov, and G. Santarelli, IEEE Tran. Micr. Theo. Tech. **59**, 2978–2986 (2011).

[6] J. Kim, J. A. Cox, J. Chen, and F. X. Kartner, Nat. Phot. **2**, 733–736 (2008).

[7] P. Ghelfi, F. Laghezza, F. Scotti, G. Serafino, A. Capria, S. Pinna, D. Onori, C. Porzi, M. Scaffardi, A. Malacarne, V. Vercesi, E. Lazzeri, F. Berizzi, and A. Bogoni, Nature **507**, 341–345 (2014).

[8] P. Gill, Philos. Trans. Royal Soc. a-Math. Phys. Eng. Sci. **369**, 4109–4130 (2011).

[9] J. Chauvin, P. Weber, J. P. Aubry, F. Lefebvre, F. Sthal, S. Galliou, E. Rubiola, and X. Vacheret, IEEE, A new generation of very high stability BVA oscillators. Proceedings of the 2007 IEEE International Frequency Control Symposium-Jointly with the 21st European Frequency and Time Forum, Vols 1-4 (2007), pp. 1261–1268.

[10] S. R. Stein and J. P. Turneaure, Pro. IEEE **63**, 1249–1250 (1975).

[11] J. G. Hartnett and N. R. Nand, C. Lu, Appl. Phys. Lett. **100**, (2012).

[12] A. G. Mann, C. Sheng, and A. N. Luiten, IEEE Tran. Inst. Measu. **50**, 519–521 (2001).

[13] S. Galliou, M. Goryachev, R. Bourquin, P. Abbe, J. P. Aubry, and M. E. Tobar, Sci. Rep-Uk **3**, (2013).

[14] A. Sen Gupta, D. A. Howe, C. Nelson, A. Hati, F. L. Walls, and J. F. Nava, IEEE Tran. Ultr. Ferro. Freq. Con. **51**, 1225–1231 (2004).

[15] E. N. Ivanov and M. E. Tobar, IEEE Tran. Ultra. Ferr. Freq. Con. **56**, 263–269 (2009).

[16] K. Watabe, S. Yanagimachi, A. Takamizawa, T. Ikegami, S. Ohshima, G. Santarelli, C. R. Locke, and J. G. Hartnett, Japa. J. Appl. Phys. **47**, 7390–7392 (2008).

[17] J. G. Hartnett, S. R. Parker, E. N. Ivanov, T. Povey, N. R. Nand, and J. M. le Floch, Elect. Lett **50**, 294–U137 (2014).

[18] Y. Y. Jiang, A. D. Ludlow, N. D. Lemke, R. W. Fox, J. A. Sherman, L. S. Ma, and C. W. Oates, Natu. Photo. **5**, 158–161 (2011).

[19] N. Hinkley, J. A. Sherman, N. B. Phillips, M. Schioppo, N. D. Lemke, K. Beloy, M. Pizzocaro, C. W. Oates, and A. D. Ludlow, Science **341**, 1215–1218 (2013).

[20] B. J. Bloom, T. L. Nicholson, J. R. Williams, S. L. Campbell, M. Bishof, X. Zhang, W. Zhang, S. L. Bromley, and J. Ye, Nature **506**, 71–75 (2014).

[21] M. Takamoto, F.-L. Hong, R. Higashi, and H. Katori, Nature **435**, 321–324 (2005).

[22] T. M. Fortier, M. S. Kirchner, F. Quinlan, J. Taylor, J. C. Bergquist, T. Rosenband, N. Lemke, A. Ludlow, Y. Jiang, C. W. Oates, and S. A. Diddams, Nat. Photo. **5**, 425–429 (2011).

[23] F. Quinlan, T. M. Fortier, M. S. Kirchner, J. A. Taylor, M. J. Thorpe, N. Lemke, A. D. Ludlow, Y. Y. Jiang, and S. A. Diddams, Opt. Lett. **36**, 3260–3262 (2011).

[24] W. Zhang, Z. Xu, M. Lours, R. Boudot, Y. Kersale, G. Santarelli, and Y. Le Coq, Appl. Phys. Lett. **96**, 211105 (2010).

[25] J. Capmany and D. Novak, Nat. Photo. **1**, 319–330 (2007).

[26] M. H. Khan, H. Shen, Y. Xuan, L. Zhao, S. J. Xiao, D. E. Leaird, A. M. Weiner, and M. H. Qi, Nat. Photo. **4**, 117–U130 (2010).

[27] L. Maleki, Nat. Photo. **5**, 728–730 (2011).

[28] F. Nabki, K. Allidina, F. Ahmad, P. V. Cicek, and M. N. El-Gamal, IEEE J. Solid-State Circ. **44**, 2154–2168 (2009).

[29] H. Lee, A. Partridge, F. Assaderaghi, and Ieee, in 2012 IEEE Int. Freq. Con. Symp. (2012).

[30] K. L. Phan, T. van Ansem, C. van der Avoort, J. T. M. van Beek, M. J. Goossens, S. Jose, R. J. P. Lander, S. Menten, T. Naass, and J. Sistermans, in Solid-State Sensors, Actuators and Microsystems (Transducers & Eurosensors XXVII), 2013 Transducers & Eurosensors XXVII: The 17th International Conference on. (IEEE, 2013), pp. 802–805.

[31] S. Grop, P. Y. Bourgeois, R. Boudot, Y. Kersale, E. Rubiola, and V. Giordano, Elect. Lett. **46**, 420–422 (2010).

[32] A. Hati, C. W. Nelson, C. Barnes, D. Lirette, T. Fortier, F. Quinlan, J. A. DeSalvo, A. Ludlow, S. A. Diddams, and D. A. Howe, IEEE Trans. Ultra. Ferr. Freq. Cont. **60**, 1796–1803 (2013).

[33] T. Kessler, C. Hagemann, C. Grebing, T. Legero, U. Sterr, F. Riehle, M. J. Martin, L. Chen, and J. Ye, Nat. Photo. **6**, 687–692 (2012).

[34] Z. Li, Y. Fu, M. Piels, H. P. Pan, A. Beling, J. E. Bowers, and J. C. Campbell, Opt. Exp. **19**, 385–390 (2011).

[35] X. J. Xie, Q. G. Zhou, K. J. Li, Y. Shen, Q. L. Li, Z. Y. Yang, A. Beling, and J. C. Campbell, Optica **1**, 429–435 (2014).

[36] F. N. Baynes, F. Quinlan, T. M. Fortier, Q. Zhou, A. Beling, J. C. Campbell, and S. A. Diddams, Optica **2**, 141–146 (2015).

[37] F. Quinlan, T. M. Fortier, H. Jiang, A. Hati, C. Nelson, Y. Fu, J. C. Campbell, and S. A. Diddams, Nat. Photo. **7**, 290–293 (2013).

[38] B. C. Young, F. C. Cruz, W. M. Itano, and J. C. Bergquist, Phys. Rev. Lett. **82**, 3799–3802 (1999).

[39] R. W. P. Drever, J. L. Hall, F. V. Kowalski, J. Hough, G. M. Ford, A. J. Munley, and H. Ward, Appl. Phys. B. **31**, 97–105 (1983).

[40] L. S. Ma, P. Jungner, J. Ye, and J. L. Hall, Opt. Lett. **19**, 1777–1779 (1994).

[41] T. M. Fortier, A. Bartels, and S. A. Diddams, Opt. Lett. **31**, 1011–1013 (2006).

[42] F. Quinlan, F. N. Baynes, T. M. Fortier, Q. G. Zhou, A. Cross, J. C. Campbell, and S. A. Diddams, Opt. Lett. **39**, 1581–1584 (2014).

[43] D. J. Jones, S. A. Diddams, J. K. Ranka, A. Stentz, R. S. Windeler, J. L. Hall, and S. T. Cundiff, Science **288**, 635–639 (2000).

[44] S. A. Diddams, D. J. Jones, J. Ye, S. T. Cundiff, J. L. Hall, J. K. Ranka, R. S. Windeler, R. Holzwarth, T. Udem, and T. W. Hansch, Phys. Rev. Lett. **84**, 5102–5105 (2000).

[45] Z. Li, H. P. Pan, H. Chen, A. Beling, and J. C. Campbell, IEEE J. Quan. Elec. **46**, 626–632 (2010).

[46] W. L. Sun, F. Quinlan, T. M. Fortier, J. D. Deschenes, Y. Fu, S. A. Diddams, and J. C. Campbell, Phys. Rev. Lett. **113**, (2014).

[47] A. Haboucha, W. Zhang, T. Li, M. Lours, A. N. Luiten, Y. Le Coq, and G. Santarelli, Opt. Lett. **36**, 3654–3656 (2011).

[48] B. R. Washburn, R. W. Fox, N. R. Newbury, J. W. Nicholson, K. Feder, P. S. Westbrook, and C. G. Jorgensen, Opt. Expr. **12**, 4999–5004 (2004).

[49] C. E. Calosso, Y. Gruson, and E. Rubiola, Ieee, 2012 IEEE Inte. Freq. Cont. Sym. (Fcs). (2012).

[50] A. Hati, C. W. Nelson, and D. A. Howe, IEEE Tran. on Ultr. Ferr. Freq. Cont. **61**, 1961–1966 (2014).

[51] R. Bara, J. M. Le Floch, M. E. Tobar, P. L. Stanwix, S. R. Parker, J. G. Hartnett, and E. N. Ivanov, IEEE Micr. Wire. Comp. Lett. **22**, 85–87 (2012).

[52] C. H. Cox, E. I. Ackerman, G. E. Betts, and J. L. Prince, IEEE Tran. Micr. Theo. Tech. **54**, 906–920 (2006).

[53] J. J. Oreilly, P. M. Lane, R. Heidemann, and R. Hofstetter, Elec. Lett. **28**, 2309–2311 (1992).

[54] H. J. Song, N. Shimizu, and T. Nagatsuma, Opt. Exp. **15**, 14901–14906 (2007).

[55] H. J. Song, N. Shimizu, T. Furuta, K. Suizu, H. Ito, and T. Nagatsuma, J. Ligh. Tech. **26**, 2521–2530 (2008).

[56] A. Hirata, M. Harada, and T. Nagatsuma, J. Ligh. Tech. **21**, 2145–2153 (2003).

[57] W. Li, W. T. Wang, W. H. Sun, L. X. Wang, and N. H. Zhu, Opt. Lett. **39**, 1201–1203 (2014).

[58] H. Ito, S. Kodama, Y. Muramoto, T. Furuta, T. Nagatsuma, and T. Ishibashi, IEEE J. Sele. Top. Quan. Elect. **10**, 709–727 (2004).

[59] J. R. Vig, IEEE Tran. Ultra. Ferr. Freq. Cont. **40**, 522–527 (1993).

[60] T. Nagatsuma, IEEE Photo. J. **6**, (2014).

[61] G. H. Qi, J. P. Yao, J. Seregelyi, S. Paquet, and C. Belisle, J. Ligh. Tech. **23**, 2687–2695 (2005).

[62] Z. Jiang, C.-B. Huang, D. E. Leaird, and A. M. Weiner, Nat. Photo. **1**, 463–463 (2007).

[63] L. C. Sinclair, I. Coddington, W. C. Swann, G. B. Rieker, A. Hati, K. Iwakuni, and N. R. Newbury, Opt. Exp. **22**, 6996–7006 (2014).

[64] E. Baumann, F. R. Giorgetta, J. W. Nicholson, W. C. Swann, I. Coddington, and N. R. Newbury, Opt. Lett. **34**, 638–640 (2009).

[65] T. Wilken, M. Lezius, T. W. Hansch, A. Kohfeldt, A. Wicht, V. Schkolnik, M. Krutzik, H. Duncker, O. Hellmig, P. Windpassinger, K. Sengstock, A. Peters, and R. Holzwarth, IEEE, in 2013 Conf. on Lase. and Electro-Opt. (2013).

[66] T. R. Schibli, K. Minoshima, F. L. Hong, H. Inaba, A. Onae, H. Matsumoto, I. Hartl, and M. E. Fermann, Opt. Lett. **29**, 2467–2469 (2004).

[67] J. Lee, K. Lee, Y. S. Jang, H. Jang, S. Han, S. H. Lee, K. I. Kang, C. W. Lim, Y. J. Kim, and S. W. Kim, Sci. Rep-Uk. **4**, (2014).

[68] D. R. Leibrandt, M. J. Thorpe, M. Notcutt, R. E. Drullinger, T. Rosenband, and J. C. Bergquist, Opt. Expr. **19**, 3471–3482 (2011).

[69] B. Argence, E. Prevost, T. Leveque, R. Le Goff, S. Bize, P. Lemonde, and G. Santarelli, Opt. Expr. **20**, 25409–25420 (2012).

[70] Q. F. Chen, A. Nevsky, M. Cardace, S. Schiller, T. Legero, S. Hafner, A. Uhde, and U. Sterr, RSI. **85**, (2014).

[71] E. Rouvalis, F. N. Baynes, X. J. Xie, K. J. Li, Q. G. Zhou, F. Quinlan, T. M. Fortier, S. A. Diddams, A. G. Steffan, A. Beling, and J. C. Campbell, J. Ligh. Tech. **32**, 3810–3816 (2014).

[72] W. Loh, A. A. S. Green, F. N. Baynes, D. C. Cole, F. J. Quinlan, H. Lee, K. J. Vahala, S. B. Papp, and S. A. Diddams, Optica **2**, 225–232 (2015).

[73] J. Alnis, A. Schliesser, C. Y. Wang, J. Hofer, T. J. Kippenberg, and T. W. Hansch, Phys. Revi. A **84**, (2011).

[74] W. Liang, V. S. Ilchenko, D. Eliyahu, A. A. Savchenkov, A. B. Matsko, D. Seidel, and L. Maleki, Natu. Commu. **6**, (2015).

[75] P. Del'Haye, A. Schliesser, O. Arcizet, T. Wilken, R. Holzwarth, and T. J. Kippenberg, Nature **450**, 1214–1217 (2007).

[76] T. J. Kippenberg, R. Holzwarth, and S. A. Diddams, Science **332**, 555–559 (2011).

[77] J. Li, X. Yi, H. Lee, S. A. Diddams, and K. J. Vahala, Science **345**, 309–313 (2014).

[78] S. B. Papp, K. Beha, P. Del'Haye, F. Quinlan, H. Lee, K. J. Vahala, and S. A. Diddams, Optica **1**, 10–14 (2014).

[79] W. Liang, D. Eliyahu, V. S. Ilchenko, A. A. Savchenkov, A. B. Matsko, D. Seidel, and L. Maleki, Natu. Commu. **6**, (2015).

[80] D. Eliyahu, W. Liang, E. Dale, A. A. Savchenkov, V. S. Ilchenko, A. B. Matsko, D. Seidel, and L. Maleki, IEEE Photo. Tech. Lett. **25**, 1535–1538 (2013).

[81] J. J. Zhang, L. Gao, and J. P. Yao, IEEE Photo. Tech. Lett. **26**, 326–329 (2014).

[82] J. F. Cliche and B. Shillue, IEEE Cont. Syst. Mag. **26**, 19–26 (2006).

[83] G. J. Schneider, J. A. Murakowski, C. A. Schuetz, S. Y. Shi, and D. W. Prather, Natu. Photo. **7**, 118–122 (2013).

[84] G. Pillet, L. Morvan, L. Menager, A. Garcia, S. Babiel, and A. Stohr, J. Ligh. Tech. **32**, 3824–3830 (2014).

[85] R. Bara-Maillet, S. R. Parker, N. R. Nand, J. M. Le Floch, and M. E. Tobar, IEEE Trans. Ultra. Ferro. Freq. Cont. **62**, 1895–1900 (2015).